CHEMISTRY OF MATERIALS

Article

pubs.acs.org/cm

Oxide-Ion Conductivity of Highly *c*-Axis-Oriented Apatite-Type Lanthanum Silicate Polycrystal Formed by Reactive Diffusion between La_2SiO_5 and $La_2Si_2O_7$

Koichiro Fukuda,*[,†] Toru Asaka,[†] Ryuta Hamaguchi,[†] Takahiro Suzuki,[†] Hideki Oka,[†] Abid Berghout,[‡] Emilie Béchade,[‡] Olivier Masson,[‡] Isabelle Julien,[‡] Eric Champion,[‡] and Philippe Thomas[‡]

[†]Department of Environmental and Materials Engineering, Nagoya Institute of Technology, Nagoya 466-8555, Japan

[‡]Science des Procédés Céramiques et de Traitements de Surface—SPCTS, UMR 6638, Centre Européen de la Céramique, 12 Rue Atlantis, 87068 Limoges Cedex, France

Supporting Information

ABSTRACT: We have successfully synthesized the highly *c*-axis-oriented polycrystals of apatite-type lanthanum silicate by the reactive diffusion technique. When the $La_2SiO_5/La_2Si_2O_7$ diffusion couples were isothermally heated at 1773−1873 K for 5−100 h, the apatite polycrystals were readily produced in the form of a layer at the interfacial boundaries. The annealed couples were characterized using optical microscopy, micro-Raman spectroscopy, X-ray diffractometry, and electron probe microanalysis. The product layers were composed of the highly *c*-axis-oriented prismatic crystallites, with their elongation directions being almost parallel to the diffusion direction. The formation of the apatite layer was controlled by volume diffusion, the overall reaction of which is described by $(10 + 6x)La_2SiO_5 + (4-3x)La_2Si_2O_7 \rightarrow 3La_{9.33+2x}(SiO_4)_6O_{2+3x}$ $(0.01 \leq x \leq 0.13)$. The apatite layer formed at 1873 K was characterized by the steady decrease of the *x*-value along the diffusion direction from 0.13 at the La_2SiO_5/apatite interface to 0.01 at the apatite/$La_2Si_2O_7$ interface. We have also prepared sandwich-type $La_2Si_2O_7/La_2SiO_5/La_2Si_2O_7$ diffusion couples and heated them at 1873 K for 100 h. The annealed couple was mechanically processed, and the thin-plate electrolyte consisting of the highly *c*-axis-oriented polycrystal was obtained. The oxide-ion conductivity was determined from the impedance spectroscopy data at 573−973 K, which steadily increased from 2.4×10^{-3} S/cm to 2.39×10^{-2} S/cm with increasing temperature. The empirical activation energy of conduction was 0.35 eV, which compares well with the calculated migration energy of 0.32 eV in a previous study.

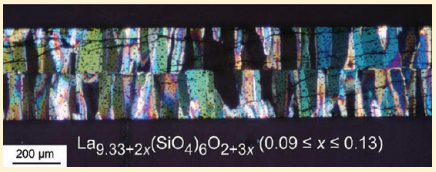

KEYWORDS: *oxide-ion conductor, lanthanum silicates, apatite, reactive diffusion, crystalline orientation*

INTRODUCTION

Apatite-type rare-earth (RE) silicates, $RE_{9.33}(SiO_4)_6O_2$, are promising materials for gas-sensing devices and electrolytes for use in solid-oxide fuel cells (SOFCs) because of the relatively high oxide-ion conductivity at moderate temperatures, as well as at low oxygen partial pressures.[1,2] The lanthanum silicate $La_{9.33}(SiO_4)_6O_2$ has exhibited higher conductivity than the other RE silicates. Nakayama et al. have prepared single crystals of $RE_{9.33}(SiO_4)_6O_2$ (RE = Pr, Nd, and Sm), which are isotypic to $La_{9.33}(SiO_4)_6O_2$, using the floating zone (FZ) method to demonstrate anisotropy of oxide-ion conduction.[3,4] The conductivity was much higher parallel to the *c*-axis than perpendicular to this direction. The theoretical results have also suggested that the oxide-ion conduction occurs along the *c*-axis via nonlinear pathways.[5−8] Thus, the highly *c*-axis-oriented materials should show high-performance conductivity. However, the FZ method is inapplicable to the growth of $La_{9.33}(SiO_4)_6O_2$ single crystals because this material is transparent in infrared light.

Okudera et al. have clarified, using a single-crystal X-ray diffraction method, that the crystal structure of $La_{9.33}(SiO_4)_6O_2$ belongs to the space group $P6_3/m$ (optically uniaxial).[9] Masubuchi et al. have confirmed, using the neutron powder diffraction method, that the crystal structures of $La_{9.33}(SiO_4)_6O_2$ and $Nd_{9.33}(SiO_4)_6O_2$ are isotypic.[10] These two structural studies are reconciled with each other on the basis of the absence of interstitial oxygen sites in the crystal lattices. Several researchers have reported the existence of excess oxide ions in the apatite-type crystal structures,[11−19] although the exact positions of these sites are still not clear.[10,20−22] The interstitial oxide ions are considered to mediate the fast oxide-ion conductivity. On the other hand, the lanthanum- and oxygen-deficient crystals show lower conductivity, as compared with $La_{9.33}(SiO_4)_6O_2$.[23] The amounts of excess and deficient oxide ions are expressed by the positive and negative values, respectively, of *x* for the general formula $La_{9.33+2x}(SiO_4)_6O_{2+3x}$. The exact range of the *x*-value, which must be dependent on the formation temperature, is still uncertain. The highest performance of oxide-ion conductivity has been reported for $La_{10}(SiO_4)_6O_3$ $(x \approx 0.33)$ among the polycrystalline materials of $La_{9.33+2x}(SiO_4)_6O_{2+3x}$; the conductivities were 2.42×10^{-4} S/cm at 573 K and 1.08×10^{-2} S/cm at 973 K.[2]

Received: October 4, 2011
Revised: November 3, 2011
Published: November 22, 2011

For the binary systems in which intermediate compounds appear as stable phases, the equilibrium phase diagrams may be experimentally determined by a reactive diffusion technique.[29] In this technique, a diffusion couple consisting of two compounds with different chemical compositions in the relevant system is annealed at the desired temperatures. During the heating process, the intermediate compound(s) will be produce in the form of a layer at the couple interface. On the basis of the phase and chemical compositions of the product phase(s), the phase stabilities in the binary systems can be established. In the La_2O_3−SiO_2 binary system, there are three compounds established so far;[30] they are La_2SiO_5 in the La_2O_3-rich region, $La_2Si_2O_7$ in the SiO_2-rich region, and apatite-type $La_{9.33+2x}(SiO_4)_6O_{2+3x}$ as the intermediate compound. To our knowledge, the reactive diffusion technique has never been used for the formation of $La_{9.33+2x}(SiO_4)_6O_{2+3x}$. We expect that the exact range of x-values at desired temperatures would be readily clarified by this technique.

Sintered polycrystals (e.g., ceramics) prepared by conventional sintering methods generally possess a randomly oriented grain structure and isotropic physical (e.g., thermoelectric, piezoelectric, pyroelectric, and magnetic) and mechanical (e.g., bending strength and fracture toughness) properties. In recent years, several techniques have made it possible to produce ceramics with grain-oriented microtextures and anisotropic properties. One of the most popular texturing methods includes the templated grain growth process, in which anisotropically shaped template particles are, before sintering, aligned by tape casting.[24,25] The other grain-alignment methods include pressing at high temperatures (hot pressing), applying magnetic field, and utilizing centrifugal force.[26−28] These fabrication processes are rather complex, and also, the orientation degrees of the textured ceramics are not always satisfactory.

In the present study, we have successfully prepared the $La_{9.33+2x}(SiO_4)_6O_{2+3x}$ polycrystalline materials by the reactive diffusion between La_2SiO_5 and $La_2Si_2O_7$ to determine the variation of x-values. Furthermore, we have found that the product apatite layers are composed of the highly c-axis-oriented polycrystals. Thus, we have prepared the electrolyte consisting of this apatite layer to show the high oxide-ion conductivity. We have consequently proposed that the reactive diffusion technique can be used as a new facile and advanced texturing method for the syntheses of highly grain-oriented ceramics.

EXPERIMENTAL SECTION

Powder Materials. Three types of powder specimens with different chemical compositions of La_2SiO_5, $La_2Si_2O_7$, and $La_{9.33}(SiO_4)_6O_2$ were prepared from reagent-grade chemicals of La_2O_3 (99.99%, Mitsuwa Chemicals Co. Ltd., Osaka, Japan) and SiO_2 (99.0%, Kishida Chemical Co. Ltd., Osaka, Japan). Hygroscopic lanthanum oxide was precalcined at 1073 K for 30 min to remove lanthanum hydroxide and/or oxycarbonate phases to obtain the appropriate amount of La_2O_3. Individual well-mixed chemicals were heated at 1873 K for 3 h, followed by quenching in air. The reaction products were slightly sintered polycrystalline materials. They were finely ground to obtain fine powder specimens. The $La_2Si_2O_7$ compound has two polymorphs; one is monoclinic (denoted by m-$La_2Si_2O_7$) and the other tetragonal. The $La_2Si_2O_7$ powder as obtained was composed exclusively of the monoclinic phase. The $La_{9.33}(SiO_4)_6O_2$ powder was used as the reference material for micro-Raman spectroscopy as mentioned below.

Diffusion Couples. Each of the powder specimens of La_2SiO_5 (0.63 g) and m-$La_2Si_2O_7$ (0.54 g) was pressed into pellets with almost the same size of ϕ 12 mm × 2 mm. These two types of pellets were stacked on top of the other to form La_2SiO_5/$La_2Si_2O_7$ diffusion couples. They were isothermally heated at three different temperatures, 1773, 1823, and 1873 K, for 5 to 100 h, followed by cooling to ambient temperature by cutting furnace power. Inert markers (platinum wires) were placed in advance at the original contact surface of the couples.

We also prepared sandwich-type diffusion couples of $La_2Si_2O_7$/La_2SiO_5/$La_2Si_2O_7$, each of which was made up of one La_2SiO_5 pellet (0.480 g) with the size of ϕ 12 mm ×0.7 mm and two m-$La_2Si_2O_7$ pellets (0.153 g each) with the size of ϕ 12 mm × 0.3 mm. They were heated at 1873 K for 100 h, followed by cooling to ambient temperature by cutting furnace power.

Optical Microscopy. The annealed couples were cut with a diamond saw to expose sections, the surfaces of which were perpendicular to or parallel to the diffusion direction. These cross sections were then mechanically ground with 800-grid SiC paper and polished with 1-μm diamond paste. Parts of them were subsequently made into thin sections and their microtextures were observed using an optical microscope.

Micro-Raman Spectroscopy. Micro-Raman spectra were obtained in the range from 100 cm^{-1} to 1000 cm^{-1} with a spectral resolution of 1 cm^{-1}, using a double-grating monochromator with a backscattering geometry (model NRS-2000, JASCO Co., Tokyo, Japan). The magnification of the objective lens was 20 times. The green line (514.5 nm) of an argon-ion laser was used for Raman spectral excitation with a power of 10 mW. Identification was made by comparison with the reference spectra, which were collected from the starting powder materials.

X-ray Powder Diffractometry. The X-ray powder diffractometry (XRPD) patterns were obtained using a diffractometer (X'Pert PRO Alpha-1, PANalytical B.V., Almelo, The Netherlands) in the Bragg−Brentano geometry, which was equipped with an incident-beam Ge(111) Johansson monochromator to obtain Cu Kα_1 radiation and a high-speed detector. The X-ray generator was operated at 45 kV and 40 mA. An automatic divergence slit was used to keep a constant illuminated length of 5 mm on the specimen surface. The beam width was 5 mm; hence, the analyzed surface area was ca. 25 mm^2. Other experimental conditions were as follows: continuous scan, experimental 2θ range from 10.0° to 90.0°, 2394 total data points, and 16 min total experimental time. The texture fraction of the apatite {00l} planes was estimated from the XRPD patterns using the Lotgering method.[31]

The Lotgering factor f_{00l} is defined as the fraction of area textured with the crystallographic plane of interest using the formula

$$f_{00l} = (P_{00l} - P_0)/(1 - P_0)$$

where

$$P_{00l} = (\Sigma I_{00l})/(\Sigma I_{hkl})$$

and

$$P_0 = (\Sigma I_{00l}{}^0)/(\Sigma I_{hkl}{}^0)$$

where I_{hkl} and $I_{hkl}{}^0$ are the intensities of the hkl peaks for the textured and for the randomly oriented sample, respectively. The entire experimental diffraction patterns were employed for the Le Bail method[32] to extract the integrated intensities using the computer program RIETAN-FP.[33] The simulated XRPD pattern was generated using this computer program for the apatite polycrystal with a completely random orientation. The structural parameters used were those determined by Okudera et al.[9]

Electron Probe Microanalysis. Concentration distribution maps for La and Si were obtained using electron probe microanalysis (EPMA) (model JXA-8900 L, JEOL). The area of analysis on the

dx.doi.org/10.1021/cm2029905 | Chem. Mater. 2011, 23, 5474−5483

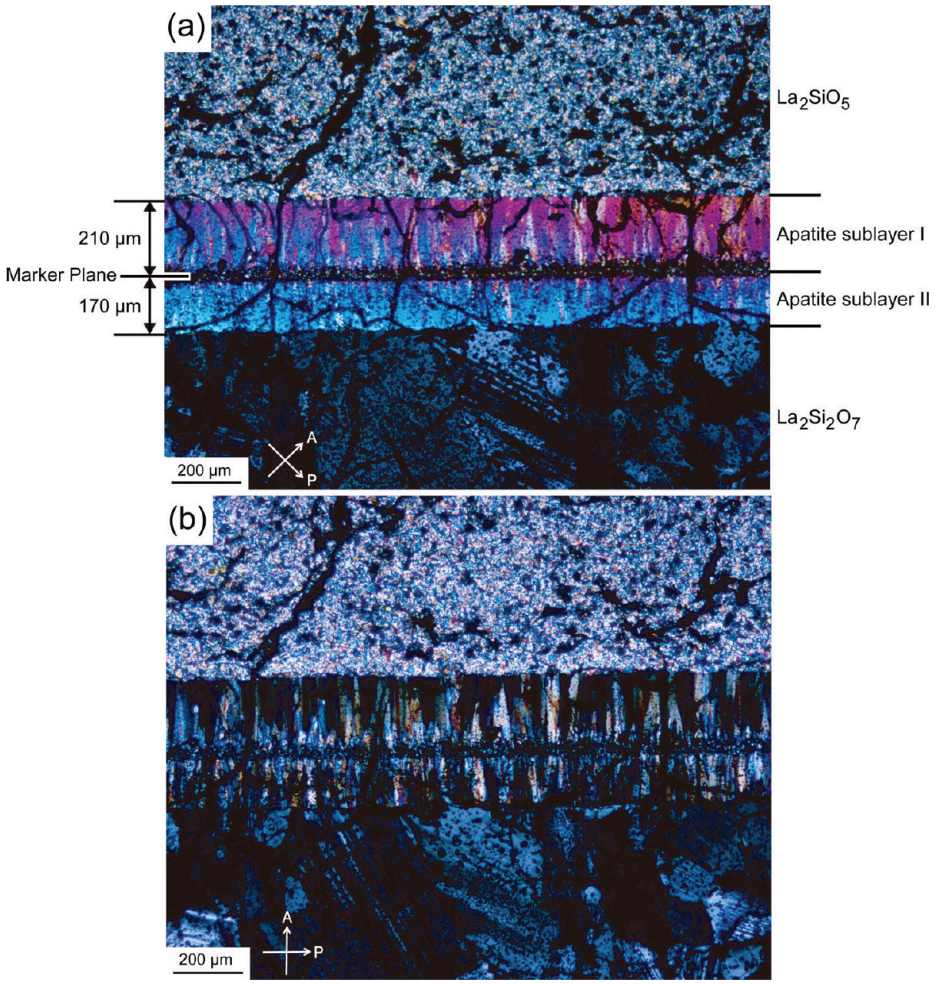

Figure 1. Optical micrographs of the $La_2SiO_5/La_2Si_2O_7$ couple annealed at 1873 K for 25 h. Thin section under crossed polars. The arrows indicate the orientations of the vibration planes of the polarizer (P) and the analyzer (A) of the microscope. The apatite crystals (optically uniaxial) are elongated parallel to the *c*-axis; hence, they exhibit straight extinction. Most of the prismatic apatite crystals are diagonal in position in (a) and in extinction position in (b). The angle of rotation between the sample positions in (a) and (b) is 45°.

polished surface was 1 mm × 1 mm with 1000 pixels × 1000 pixels, and the accelerating voltage was 20 kV, and the probe current was 2.0×10^{-8} A. The quantitative line analysis was made with an 1 μm specimen shift. The La_2SiO_5 crystal grain was used for the standard material for La and Si. The corrections were made by ZAF routines.

Impedance Spectroscopy. The annealed sandwich-type diffusion couple (ca. 1.4 mm in thickness) was ground with 800-grid SiC paper and polished with 1-μm diamond paste to obtain the thin-plate electrolyte (ca. 0.38 mm in thickness). Electrodes were subsequently prepared by coating both plate faces with a platinum paste, and the plates were then heated at 1273 K to decompose the paste and harden the Pt residue. Impedance spectroscopy data were collected in air during heating from 573 to 973 K, using an impedance analyzer (model 3532-80, HIOKI E. E. Co., Nagano, Japan) over the frequency range from 4 Hz to 1 MHz.

RESULTS AND DISCUSSION

Highly *c*-Axis-Oriented Apatite Polycrystals Formed in Annealed $La_2SiO_5/La_2Si_2O_7$ Couples. The apatite-type lanthanum silicate layers were successfully formed at the interface of $La_2SiO_5/La_2Si_2O_7$ diffusion couples. The typical microtexture, viewed perpendicular to the diffusion direction, is shown in Figure 1. There are three distinct regions separated by planar boundaries, the phase and chemical compositions of which were identified by the Raman spectra (see Figure S1 in the Supporting Information) and concentration distribution maps (see Figure S2 in the Supporting Information); the three regions were composed of La_2SiO_5, apatite, and *m*-$La_2Si_2O_7$. The product apatite layer was further demarcated into two adjacent sublayers by the marker plane, where the Pt markers were introduced in advance between the original couple halves (see Figure S3 in the Supporting Information). The marker planes were easily recognized, even for the Pt marker-free couples, because small voids (<ϕ 1 μm) were eventually accumulated along the planes. For all annealed couples, the marker planes were flat and located within the apatite layers. The sublayer on the La_2SiO_5 side (denoted by I as shown in Figure 1) was necessarily thicker than that on the $La_2Si_2O_7$ side (denoted by II). The optical microscopic observation revealed that both sublayers I and II were made up of aggregates of prismatic crystallites. It should be noted that these apatite crystallites are fairly close to the extinction position under crossed polars, indicating that they are highly oriented so that their elongation directions are almost parallel to the diffusion direction (Figure 1).

The simulated XRPD pattern of randomly oriented apatite crystallites (Figure 2a) shows the highest intensity of 211 ($2\theta \approx 30.7°$). On the other hand, a marked increase of 00*l* (l = 2, 4, and 6) reflections was observed for the XRPD pattern taken on

dx.doi.org/10.1021/cm2029905 | *Chem. Mater.* 2011, 23, 5474–5483

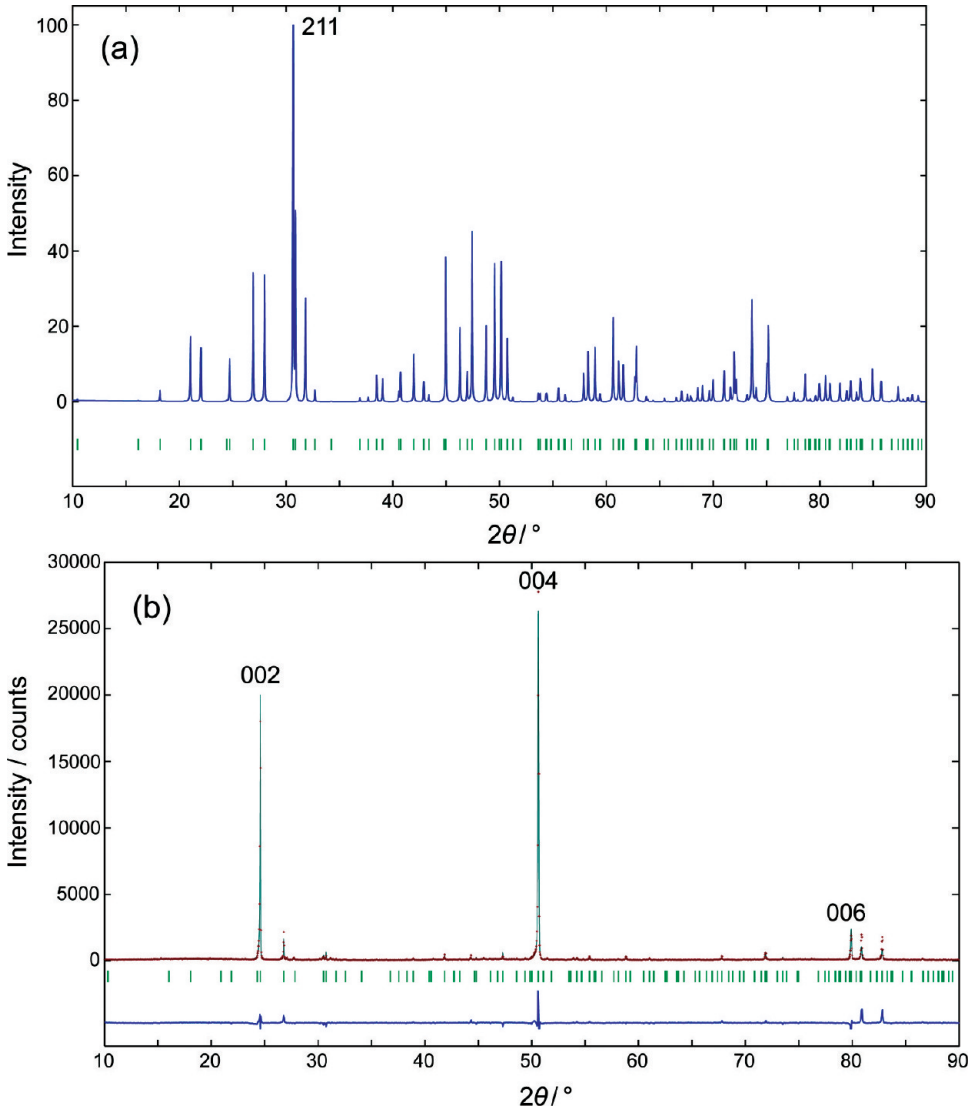

Figure 2. Simulated and observed X-ray powder diffraction patterns of apatite polycrystals. (a) Simulated pattern for randomly oriented $La_{9.33}(SiO_4)_6O_2$ crystals. Vertical bars indicate the positions of possible Bragg reflections. (b) Comparison of the observed diffraction pattern (red symbol: +) taken on the section surface, which is perpendicular to the diffusion direction of the $La_2SiO_5/La_2Si_2O_7$ couple annealed at 1873 K for 25 h, with the corresponding calculated pattern (green solid line). The difference curve is shown in the lower part of the diagram.

the section surface that is perpendicular to the diffusion direction, indicating that the individual crystals are elongated along the *c*-axis (Figure 2b). The f_{00l}-value of the apatite layer, which was formed by annealing at 1873 K for 25 h, was 0.81. Thus, apatite sublayers I and II have been found to be composed of the highly *c*-axis-oriented prismatic crystallites. Because apatite crystal is optically uniaxial (i.e., the optical axis is parallel to the crystallographic *c*-axis), all of the crystallites will be in the extinction position at the same time under crossed polars, if their *c*-axis orientations are exactly parallel to one another. Actually, some of the crystallites in sublayers I and II satisfy this condition. However, the others are in the different crystallographic orientations, which can be readily recognized under the microscope by the difference in extinction positions. We measured the rotation angles between the extinction positions of various crystallite pairs to find that the maximum angle was 13.5°.

Chemical Composition and Formation Mechanism of the Apatite Layer. The concentration profile across an about 380 μm thick apatite layer, which was formed during heating at 1873 K for 25 h, is shown in Figure 3. The average La/Si ratio of the La_2SiO_5 region was 2.005(2) and that of the $La_2Si_2O_7$ region was 0.993(4). These values follow, within the error of measurement, exact stoichiometric relationships. Thus, the quantitative analysis of the apatite layer must be highly accurate and reliable. The La/Si ratio of the apatite layer showed, without detectable discontinuity at the marker-plane boundary, a steady decrease from 1.600(3) on the La_2SiO_5/apatite interface to 1.558(6) on the apatite/$La_2Si_2O_7$ interface. The chemical variation of the apatite crystals was deduced from this change of La/Si ratio and represented by $0.01(2) \leq x \leq 0.13(1)$ of the general formula $La_{9.33+2x}(SiO_4)_6O_{2+3x}$. At the marker-plane boundary, the La/Si ratio was 1.577(4), corresponding to $x = 0.06(1)$. As a result, the chemical variation along the diffusion direction of sublayer I is $0.06(1) \leq x \leq 0.13(1)$ and that of sublayer II is $0.01(2) \leq x \leq 0.06(1)$. Because the *x*-values of the individual crystallites are necessarily larger for sublayer I than for sublayer II, the former sublayer would be favored in oxide-ion conductivity over the latter.

dx.doi.org/10.1021/cm2029905 | *Chem. Mater.* 2011, 23, 5474–5483

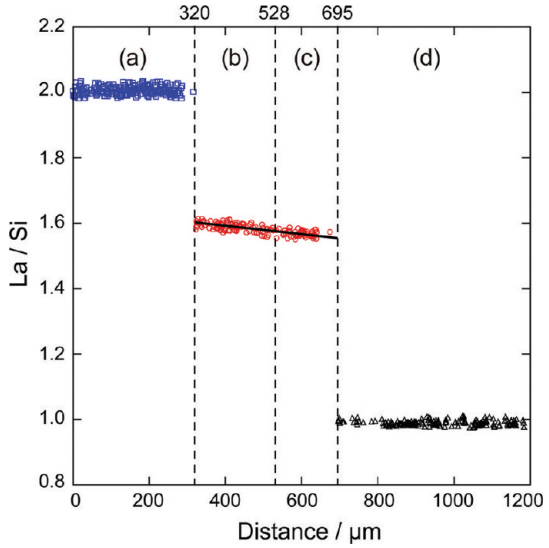

Figure 3. Step line scan analysis across the regions of (a) La_2SiO_5, (b) apatite sublayer I, (c) apatite sublayer II, and (d) $La_2Si_2O_7$, taken on the section surface of the $La_2SiO_5/La_2Si_2O_7$ couple annealed at 1873 K for 25 h. The La/Si ratio of apatite (= y) steadily decreases with increasing distance (= x/μm) from the La_2SiO_5/apatite interface. The linear fit suggests $y = 1.636(4) - 0.000112(8)x$ ($320 \le x \le 695$).

The product apatite sublayers I and II most probably grow differently from the two interfaces and meet at the marker plane. At the La_2SiO_5/apatite interface, the apatite-phase nucleates and grows by the loss of the La_2O_3 component from La_2SiO_5 and by the reaction of La_2SiO_5 with the SiO_2 component, which was released from $La_2Si_2O_7$. In terms of chemical reactions, the formation process of sublayer I can be described by the two following equations:

$$18La_2SiO_5 - (4 - 3x)La_2O_3 \rightarrow 3La_{9.33+2x}(SiO_4)_6O_{2+3x} \quad (1)$$

and

$$(14 + 3x)La_2SiO_5 + (4 - 3x)SiO_2 \rightarrow 3La_{9.33+2x}(SiO_4)_6O_{2+3x} \quad (2)$$

where $0.06(1) \le x \le 0.13(1)$.

On the other hand, at the apatite/$La_2Si_2O_7$ interface, the apatite phase nucleates and grows by the reaction of $La_2Si_2O_7$ with the La_2O_3 component, released from La_2SiO_5, and by the loss of the SiO_2 component from $La_2Si_2O_7$. These reactions in sublayer II can be expressed by the following:

$$9La_2Si_2O_7 + (5 + 3x)La_2O_3 \rightarrow 3La_{9.33+2x}(SiO_4)_6O_{2+3x} \quad (3)$$

and

$$(14 + 3x)La_2Si_2O_7 - (10 + 6x)SiO_2 \rightarrow 3La_{9.33+2x}(SiO_4)_6O_{2+3x} \quad (4)$$

where $0.01(2) \le x \le 0.06(1)$.

Both components La_2O_3 and SiO_2 are therefore required to interdiffuse in the growing apatite layer. With reactions 1 and 3, the amount of La_2O_3 component transferring per unit area through the marker plane is exactly the same; hence, we obtain

$$(10 + 6x)La_2SiO_5 + (4 - 3x)La_2Si_2O_7 \rightarrow 3La_{9.33+2x}(SiO_4)_6O_{2+3x} \quad (5)$$

where $0.01(2) \le x \le 0.13(2)$.

This equation describes the formation reaction of the overall apatite layer at the interface of La_2SiO_5 and $La_2Si_2O_7$. We obtain the same reaction formula eq 5 from eqs 2 and 4, taking into consideration of the mass balance on SiO_2 component.

Growth Behavior of Product Apatite Layer. The planar morphology was observed in all annealed couples for the interface boundaries La_2SiO_5/apatite and apatite/$La_2Si_2O_7$. These boundaries and marker plane were almost parallel to one another; hence, the average thickness l_i of apatite sublayer i (= I and II) can be evaluated by the equation:

$$l_i = A_i/w_i$$

where A_i is the total area of the apatite sublayer i and w_i is the total length of the apatite sublayer i parallel to the interface.[34] For example, the thickness of sublayer I (= l_I) in Figure 1 was, after annealing at 1873 K for 25 h, ca. 210 μm and that of sublayer II (= l_{II}) was ca. 170 μm, with the average total thickness ($l_I + l_{II}$) being ca. 380 μm. At each annealing temperature, the l_i-value steadily increased with increasing annealing time (t). A plot of log l_i vs log t gave straight lines (Figure 4), which implies that l_i is

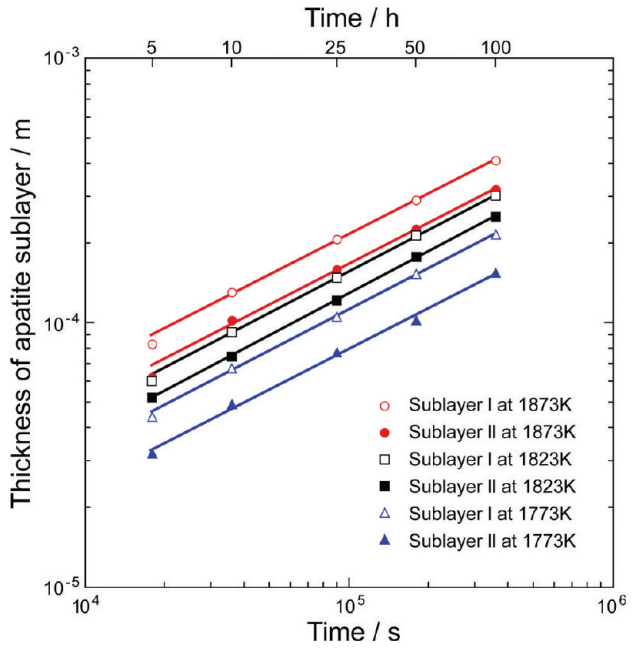

Figure 4. Thickness l_i of apatite sublayer i (= I and II) with time for the $La_2SiO_5/La_2Si_2O_7$ couples annealed at 1773–1873 K for 5–100 h.

described as a power function of t as follows:

$$l_i = K_i(t/t_0)^n$$

where t_0 is unit time (= 1 s) and K_i is a proportionality coefficient.[34] We determined the K_i-values and exponent n-values with annealing temperatures by the least-squares method (Table 1). All of the n-values with three different temperatures have been found to be close to 0.5, indicating that the average thickness of apatite sublayer almost increases parabolically with time. This implies that the growth of each apatite sublayer at

dx.doi.org/10.1021/cm2029905 | Chem. Mater. 2011, 23, 5474–5483

Table 1. K_i- and n-Values with Annealing Temperatures[a]

	apatite sublayer I		apatite sublayer II	
temp., K	K_I, m	n	K_{II}, m	n
1873	$6.0(8) \times 10^{-7}$	0.51(1)	$4.5(8) \times 10^{-7}$	0.51(1)
1823	$3.9(4) \times 10^{-7}$	0.521(8)	$2.9(2) \times 10^{-7}$	0.528(5)
1773	$2.9(3) \times 10^{-7}$	0.516(8)	$2.2(6) \times 10^{-7}$	0.51(2)

[a]Determined by the least-squares method.

these temperatures is controlled by volume diffusion.[29,34] We plotted the logarithms of K_i against the reciprocal of annealing temperature (Figure 5) to find that the temperature

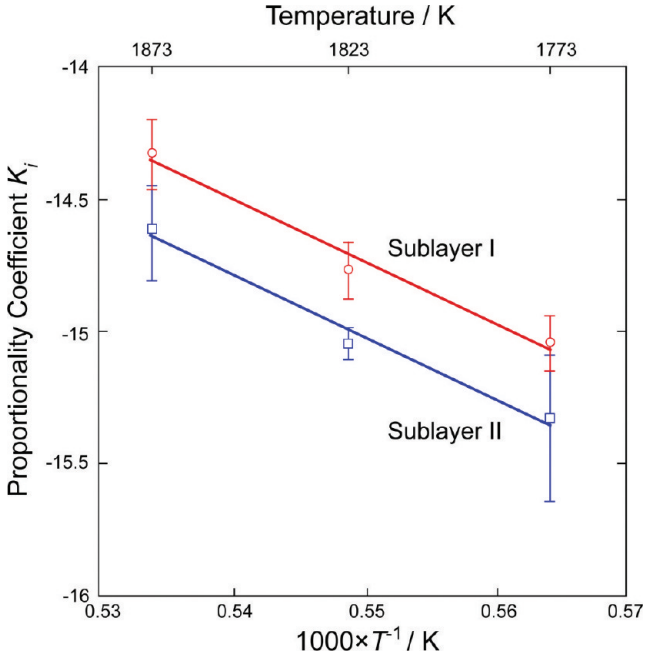

Figure 5. Proportionality coefficient K_i of apatite sublayer i (= I and II) with the reciprocal of temperature for the $La_2SiO_5/La_2Si_2O_7$ couples annealed at 1773−1873 K.

dependence of K_i was well expressed by the following equation:

$$K_i = K_i^0 \exp(-Q_i/kT)$$

where Q_i is the activation energy for the growth of sublayer i, K_i^0 is the pre-exponential factor, and k is Boltzmann constant. The Q_i- and K_i^0-values were determined from a least-squares method to be Q_I = 198 ± 30 kJ/mol and K_I^0 = 0.19 m for the sublayer I, and Q_{II} = 198 ± 27 kJ/mol and K_{II}^0 = 0.14 m for the sublayer II. Both Q_I- and Q_{II}-values have been found to be nearly equal to 200 kJ/mol, within the error limits.

The growth of the apatite layers would depend on the rate of two processes: the interdiffusion of La_2O_3 and SiO_2 components to the growing layer interface (volume diffusion process), followed by their incorporation onto the surface of the apatite phase (interfacial process). In such sequential reactions, the overall reaction rate is determined by the slowest step, and hence, an experimentally determined activation energy most probably refers to this process.[35] Because the growth of the apatite layer is diffusion controlled, as mentioned previously, both Q_I and Q_{II} would correspond to the activation energies of interdiffusion in the apatite sublayers. Although individual $La_{9.33+2x}(SiO_4)_6O_{2+3x}$ crystals in the apatite sublayers have the chemical variation with $0.06 \leq x \leq 0.13$ for sublayer I and $0.01 \leq x \leq 0.06$ for sublayer II, their crystal structures are almost the same, which accounts for the close values between Q_I and Q_{II}. The larger value of K_I^0, as compared with K_{II}^0, is responsible for the growth rate for the sublayer I being higher than that for the sublayer II.

Microtexture of Annealed $La_2Si_2O_7/La_2SiO_5/La_2Si_2O_7$ Sandwich-Type Couples. The annealed sandwich-type couple is characterized by the presence of two marker planes and the absence of La_2SiO_5 regions (Figure 6). This microtexture indicates that the former La_2SiO_5 region was completely converted to the apatite sublayer I, as a result of the sufficient supplementation of the SiO_2 component from the $La_2Si_2O_7$ regions. At the initial stage of annealing the apatite crystallites will start to nucleate on both sides of the $La_2SiO_5/La_2Si_2O_7$ interfacial boundaries and, on further heating, successively grow toward the center of the La_2SiO_5 region until they eventually contact each other to form the grain/grain interfacial contact boundary, as indicated by arrows in Figure 6b. This planar boundary, which is perpendicular to the diffusion direction, macroscopically divides the annealed couple into two parts.

The region of sublayer I (ca. 655 μm in thickness) in the annealed sandwich-type couple shows the relatively low concentrations of voids and microcracks, as compared with those of sublayers II on the apatite/$La_2Si_2O_7$ interfacial boundaries (Figure 6). In addition, sublayer I would be favored in oxide-ion conductivity over sublayer II, as mentioned previously. We mechanically polished both sides of the annealed couple surface and completely removed the regions of sublayer II to obtain the thin-plate electrolyte (ca. 380 μm in thickness) consisting exclusively of the region of sublayer I. This procedure can be followed with the naked eye, as the region of sublayer I is pale green and that of sublayer II is white. Because the prismatic apatite crystallites are almost parallel and compacted together in the thin plate, it displays an image adjacent to its other side (Figure 7).

After the impedance measurement, as described below, we prepared the thin section of the electrolyte, the polished surface of which is perpendicular to the electrode/electrolyte interface (Figure 8). We measured the rotation angles between the extinction positions of various crystallite pairs to find that the maximum angle was 13.2°, which is comparable to that determined for the annealed $La_2SiO_5/La_2Si_2O_7$ couple. Accordingly, the f_{00l}-value of the present electrolyte would be also ca. 0.8.

We polished both sides of the annealed couple surface equally, and hence, the grain/grain interfacial boundary is located almost at the center of the thin-plate electrolyte (Figure 8). The apatite sublayer I, with the chemical formula $La_{9.33+2x}(SiO_4)_6O_{2+3x}$, in the sandwich-type couple was formed during annealing at 1873 K; hence, there must be almost the same chemical gradient of the x-value from 0.06 at the sublayer I/sublayer II interfacial boundaries to 0.13 at the grain/grain interfacial contact boundary, as confirmed in the $La_2SiO_5/La_2Si_2O_7$ couple annealed at 1873 K. Because the lower x-value regions of the sublayer I were eliminated by 42% (= 100[(655−380)/655]) in depth direction after polishing, the x-value at the polished surface on both sides of thin-plate electrolyte must be ca. 0.09 (= 0.06 + (0.13 − 0.06)0.42). As a result, the electrolyte most probably shows the gradual increase of the x-value from 0.09 at the surface to 0.13 at the interior.

dx.doi.org/10.1021/cm2029905 | Chem. Mater. 2011, 23, 5474−5483

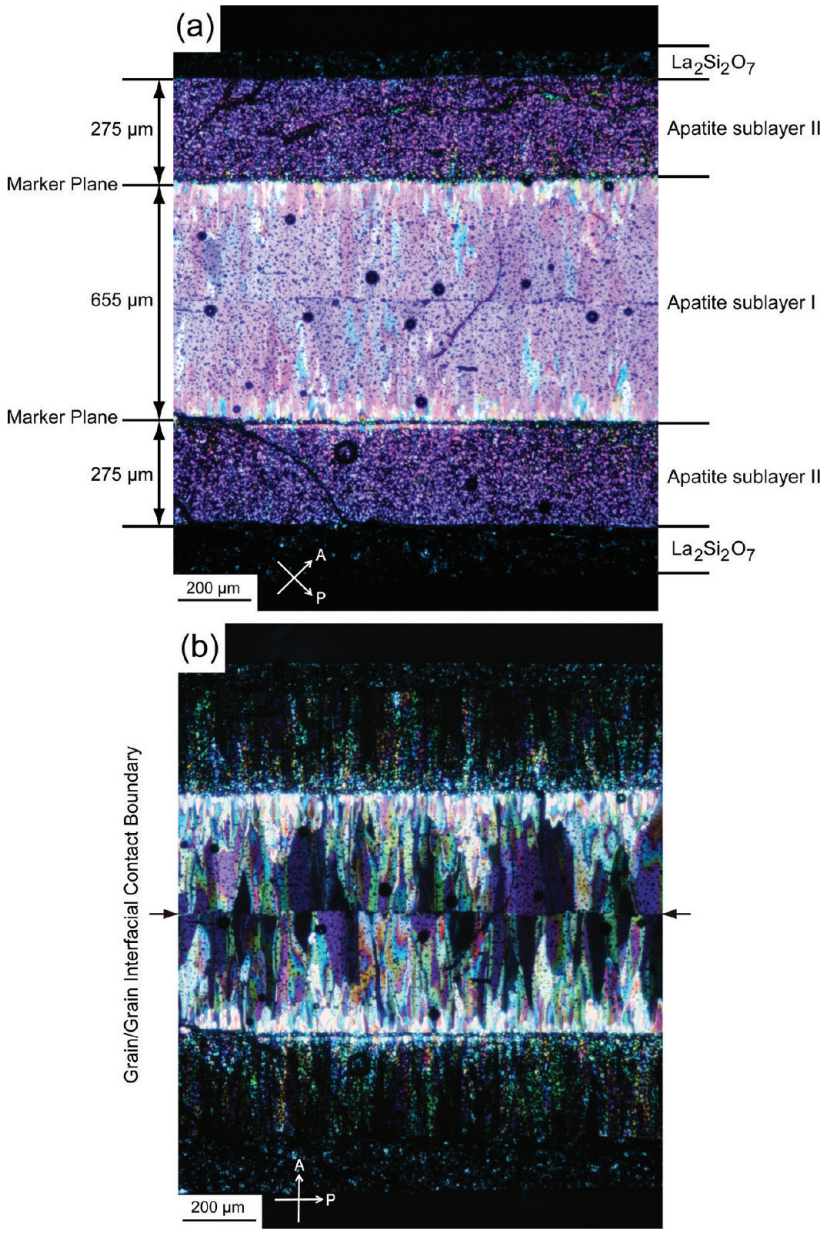

Figure 6. Optical micrographs of $La_2Si_2O_7/La_2SiO_5/La_2Si_2O_7$ sandwich-type couple annealed at 1873 K for 100 h. Thin section under crossed polars. The white arrows indicate the orientations of the vibration planes of the polarizer (P) and the analyzer (A) of the microscope. The grain/grain interfacial contact boundary is indicated by black arrows. The apatite crystals (optically uniaxial) are elongated parallel to the *c*-axis; hence, they exhibit straight extinction. Most of the prismatic apatite crystals are in a diagonal position in (a) and in an extinction position in (b). The angle of rotation between the sample positions in (a) and (b) is 45°.

Impedance Spectroscopy and Oxide-Ion Conductivity. The impedance spectra were analyzed by a nonlinear least-squares fitting method using equivalent circuits with ZView software.[36] In the circuits normally adopted for ceramics materials, the elements corresponding to bulk (b), grain boundary (gb) and electrode (e) are connected in series.[37] However, in our preliminary analysis of the present impedance spectra, there was an additional response at the frequency region between those of grain boundary and electrode. Thus, we have adopted the equivalent circuit with additional resistive and reactive components (ad) as $(R_b)(R_{gb}Q_{gb})(R_{ad}Q_{ad})(R_eQ_e)$, where R is the resistance in parallel, with a pseudocapacitance Q.[38] In general, the geometric capacitance (C) values and their possible interpretations are 10^{-11} to 10^{-8} F/cm for C_{gb} and 10^{-7} to 10^{-5} F/cm for C_e.[39] Because the present electrolyte of $La_{9.33+2x}(SiO_4)_6O_{2+3x}$ ($0.09 \leq x \leq 0.13$) is highly *c*-axis oriented, the obtained R_b-value must be of the bulk resistance almost along the *c*-axis.

The impedance diagram at 573 K exhibits one incomplete semicircle at high frequency and two overlapping semicircles at the lower frequency. The fitting result and the deconvolution of different contributions are, respectively, displayed in a blue solid line and red dashed-line semicircles in Figure 9a. The observed arc at high frequency can be identified as the grain boundary response with $C_{gb} = 5.2(9) \times 10^{-9}$ F/cm. The other two semicircles correspond to the contributions of the $R_{ad}Q_{ad}$ element, with $C_{ad} = 2.7(1) \times 10^{-7}$ F/cm at middle frequency, and the R_eQ_e element, with $C_e = 1.3(1) \times 10^{-6}$ F/cm at low frequency. The bulk resistance is extracted from the high frequency intercept of the grain boundary semicircle. The

dx.doi.org/10.1021/cm2029905 | *Chem. Mater.* 2011, 23, 5474–5483

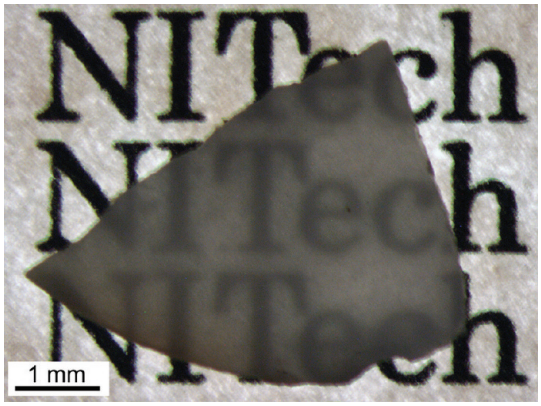

Figure 7. Optical photograph showing the transparency of $La_{9.33+2x}(SiO_4)_6O_{2+3x}$ ($0.09 \leq x \leq 0.13$) polycrystalline electrolyte, ca. 0.38 mm thick. Transmitted light.

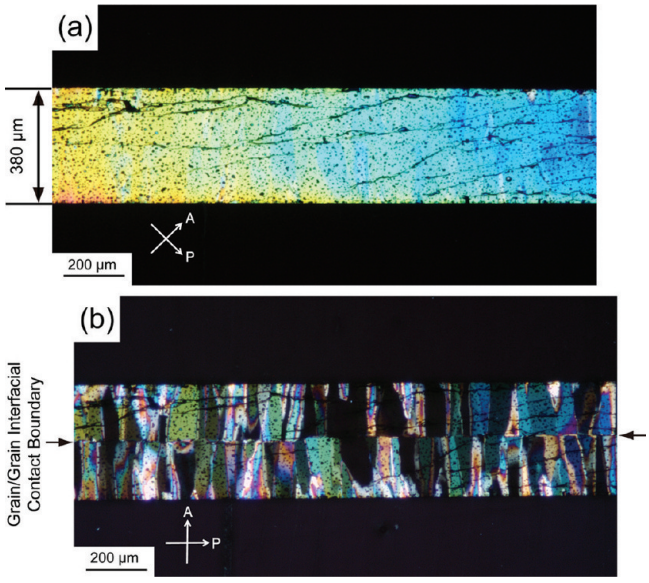

Figure 8. Optical micrographs of the thin-plate electrolyte, ca. 0.38 mm thick, viewed along the electrode/electrolyte interface. Thin section under crossed polars. The arrows indicate the orientations of the vibration planes of the polarizer (P) and the analyzer (A) of the microscope. Most of the prismatic apatite crystals are in a diagonal position in (a) and in an extinction position in (b). The angle of rotation between the sample positions in (a) and (b) is 45°. The thin-plate electrolyte consists exclusively of the apatite sublayer I. The grain/grain interfacial contact boundary, which is almost parallel to the electrode/electrolyte interface, divides the present electrolyte into two parts.

present C_{gb}- and C_e-values are in fair agreement with those determined in previous studies for $La_{9.33+2x}(SiO_4)_6O_{2+3x}$ polycrystals and ceramics materials.[39−42] The C_{ad}-value has been found to be 2 orders of magnitude larger than that of the grain boundary. As mentioned previously, the grain/grain interfacial contact boundary, which is almost parallel to the electrode/electrolyte interface, macroscopically divides the present electrolyte into two parts. The impedance response corresponding to the $R_{ad}Q_{ad}$ element must be caused by this planar boundary.

With increasing temperature, each polycrystalline region separated by the grain/grain interfacial contact boundary showed a tendency to behave like a single crystal; the grain-boundary

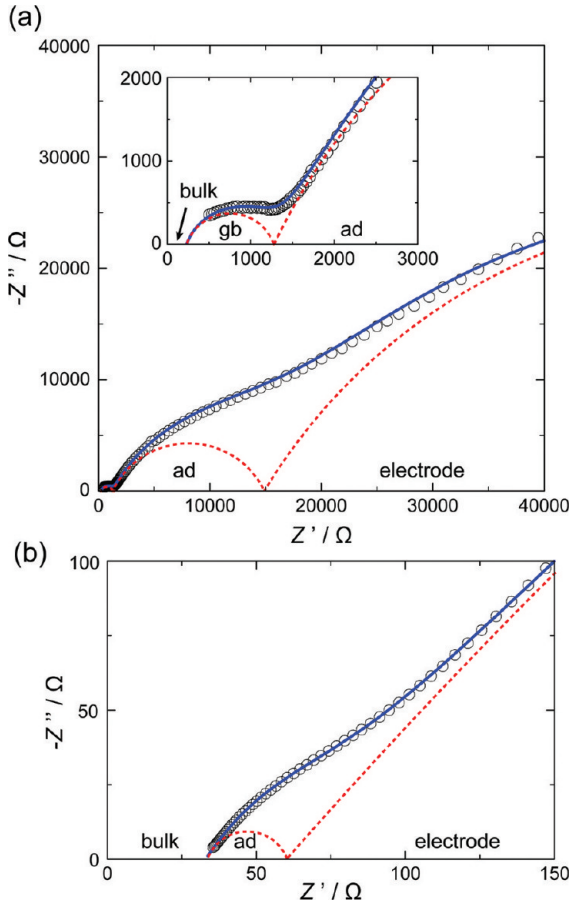

Figure 9. Nyquist plots of the $La_{9.33+2x}(SiO_4)_6O_{2+3x}$ ($0.09 \leq x \leq 0.13$) polycrystalline electrolyte. Data collected at (a) 573 K and (b) 873 K. The impedance spectra were analyzed by a nonlinear least-squares fitting method using equivalent circuits, in which the four types of elements corresponding to bulk, grain boundary (gb), additional response (ad), and electrode are connected in series. The fitting results and the deconvolution of different contributions are displayed in blue solid lines and red dashed-line semicircles, respectively.

semicircle progressively became smaller and eventually disappeared at 873 K (see Figure S4 in the Supporting Information). Thus, we adopted the $(R_{gb}Q_{gb})$-free equivalent circuit of $(R_b)(R_{ad}Q_{ad})(R_eQ_e)$ with 873 K $\leq T \leq$ 973 K. The impedance response at, for example, 873 K (Figure 9(b)) consists of a relatively small semicircle of $R_{ad}Q_{ad}$ element (C_{ad} = $2.2(2) \times 10^{-6}$ F/cm) dominated by a large semicircle due to the electrode/electrolyte interfaces ($C_e = 3.2(5) \times 10^{-5}$ F/cm). The bulk resistance is extracted from the high frequency intercept of the former semicircle. With increasing temperature from 573 to 973 K, the bulk conductivity almost along the *c*-axis (σ) steadily increased from $2.4(1) \times 10^{-3}$ S/cm to $2.39(1) \times 10^{-2}$ S/cm. These conductivities are, when compared at the same temperature, more than twice those determined for the $La_{10}(SiO_4)_6O_3$ ($x \approx 0.33$) polycrystal.[2]

The oxide-ion conductivity is thermally activated and described by

$$\sigma T = \sigma_0 \exp(-E_a/kT)$$

where E_a is the empirical activation energy, σ_0 is the pre-exponential factor, and k is Boltzmann constant. The Arrhenius plot of σ is linear over the temperature range examined

dx.doi.org/10.1021/cm2029905 | *Chem. Mater.* 2011, 23, 5474−5483

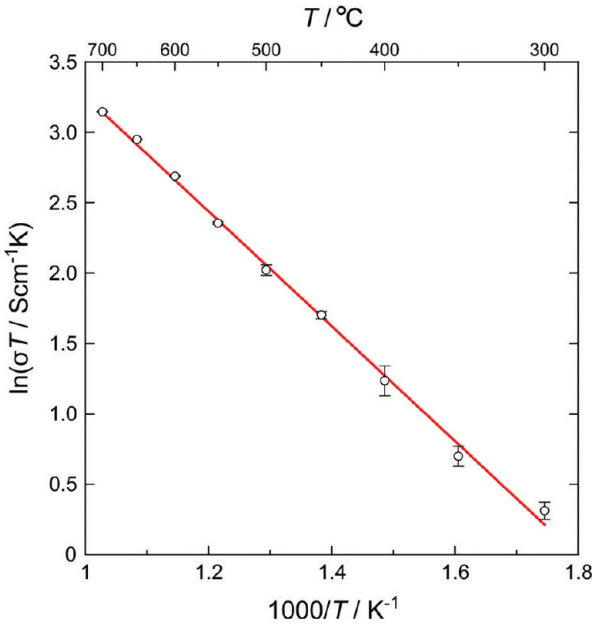

Figure 10. Arrhenius plot of the bulk conductivity almost along the *c*-axis for $La_{9.33+2x}(SiO_4)_6O_{2+3x}$ ($0.09 \leq x \leq 0.13$).

(Figure 10), and hence, the activation energy was determined from the slope to be 33.8(7) kJ/mol (= 0.350(7) eV). This value is useful to identify the temperature dependence of different conduction mechanisms. Actually, the present E_a-value is in good agreement with the theoretical migration energy of 0.32 eV, which has been evaluated by Béchade et al. for the oxide-ion conduction along the *c*-axis in $La_{9.33+2x}(SiO_4)_6O_{2+3x}$.[8] Kim et al. have analyzed the impedance spectra of $La_{10.05}(SiO_4)_6O_{3.125}$ (x = 0.375) polycrystalline material to derive the similar activation energy of 0.33 eV.[43]

In previous studies, some of the Arrhenius plots of oxide-ion conductivity of apatite-type RE silicates showed marked changes in slope at critical temperatures (T_c).[2−4,44] This implies that the oxide-ion conduction may involve at least two consecutive mechanisms above and below T_c, each with its own activation energy. The similar activation energies of 30 kJ/mol (≈ 0.31 eV)[4] and 36.8 kJ/mol (≈ 0.38 eV)[2] have been reported above T_c for the $Nd_{9.33}(SiO_4)_6O_2$ single crystal along the *c*-axis (T_c = 573 K) and $La_{10}(SiO_4)_6O_3$ ($x \approx 0.33$) polycrystalline material (T_c = 723 K), respectively. The slope changes in Arrhenius plots have been also recognized for the other oxide-ion conductors, such as $Ce_{0.9}Gd_{0.1}O_{1.95}$ and doped $LaGaO_3$, the charge carriers of which are oxygen vacancies.[45,46] As Higuchi et al. confirmed that the SOFCs using the electrolyte of $La_{9.7}(SiO_4)_6O_{2.55}$ (x = 0.183) actually operated at 673−1073 K,[47] the conducting species of the present electrolyte over the entire temperature range should be the interstitial oxide ions. Further work is necessary to elucidate the difference in the conduction mechanism of apatite-type RE silicates above and below T_c. From a practical viewpoint, it is required to further improve the oxide-ion conductivity of the present polycrystalline electrolytes in order to apply them to SOFCs, which operate at moderate temperatures. In addition to the present texturing method, the doping of foreign elements into the La and/or Si sites[11,12,48−53] of the polycrystals would remarkably enhance the conductivity.

CONCLUSION

We successfully prepared the apatite-type lanthanum silicate polycrystals by reactive diffusion between La_2SiO_5 and $La_2Si_2O_7$. The chemical composition of the product apatite layer, represented by $La_{9.33+2x}(SiO_4)_6O_{2+3x}$, was characterized by the steady decrease of the x-value from 0.13(1) on the La_2SiO_5/apatite interface to 0.01(2) on the apatite/$La_2Si_2O_7$ interface. The formation of apatite at 1773−1873 K was controlled by the interdiffusion of La_2O_3 and SiO_2 components within the growing apatite layer. The activation energy of this volume-diffusion process was *ca.* 200 kJ/mol. The highly *c*-axis-oriented polycrystalline material with $0.09 \leq x \leq 0.13$ showed the oxide-ion conductivity ranging from $2.4(1) \times 10^{-3}$ S/cm at 573 K to $2.39(1) \times 10^{-2}$ S/cm at 973 K, with the empirical activation energy being 33.8(7) kJ/mol (= 0.350(7) eV). The solid−solid reactive diffusion technique could be widely applicable to the syntheses of highly grain-oriented ceramics as a new facile texturing method.

ASSOCIATED CONTENT

Supporting Information

Figures of micro-Raman spectra, EPMA images, optical micrographs, and a series of Nyquist plots. This material is available free of charge via the Internet at http://pubs.acs.org.

AUTHOR INFORMATION

Corresponding Author

*E-mail: fukuda.koichiro@nitech.ac.jp.

ACKNOWLEDGMENTS

This research was supported by a Grant-in-Aid for Scientific Research (No. 23656399) from the Japan Society for the Promotion of Science. Thanks are due to Mr. H. Yoshida (Department of Earth and Planetary Science, the University of Tokyo) for his technical assistance in EPMA and Associate Professor M. Nakayama (Nagoya Institute of Technology) for his assistance in impedance modeling and data processing.

REFERENCES

(1) Nakayama, S.; Kageyama, T.; Aono, H.; Sadaoka, Y. *J. Mater. Chem.* **1995**, *5*, 1801.
(2) Nakayama, S.; Sakamoto, M. J. *J. Eur. Ceram. Soc.* **1998**, *18*, 1413.
(3) Nakayama, S.; Highchi, M. *J. Mater. Sci. Lett.* **2001**, *20*, 913.
(4) Nakayama, S.; Sakamoto, M.; Higuchi, M.; Kodaira, K.; Sato, M.; Kakita, S.; Suzuki, T.; Itoh, K. *J. Eur. Ceram. Soc.* **1999**, *19*, 507.
(5) Jones, A.; Slater, P. R.; Islam, M. S. *Chem. Mater.* **2008**, *20*, 5055.
(6) Islam, M. S.; Tolchard, J. R.; Slater, P. R. *Chem. Commun.* **2003**, *13*, 1486.
(7) Tolchard, J. R.; Islam, M. S.; Slater, P. R. *J. Mater. Chem.* **2003**, *13*, 1956.
(8) Béchade, E.; Masson, O.; Iwata, T.; Julien, I.; Fukuda, K.; Thomas, P.; Champion, E. *Chem. Mater.* **2009**, *21*, 2508.
(9) Okudera, H.; Masubuchi, Y.; Kikkawa, S.; Yoshiasa, A. *Solid State Ionics* **2005**, *176*, 1473.
(10) Masubuchi, Y.; Higuchi, M.; Takeda, T.; Kikkawa, S. *Solid State Ionics* **2006**, *177*, 263.
(11) Yoshioka, H.; Nojiri, Y.; Tanase, S. *Solid State Ionics* **2008**, *179*, 2165.
(12) León-Reina, L.; Losilla, E. R.; Martínez-Lara, M.; Bruque, S.; Lolbet, A.; Sheptyakow, D. V.; Aranda, M. A. G. *J. Mater. Chem.* **2005**, *15*, 2489.
(13) León-Reina, L.; Porras-Vázquez, J. M.; Losilla, E. R.; Aranda, M. A. G. *Solid State Ionics* **2006**, *177*, 1307.

(14) León-Reina, L.; Porras-Vázquez, J. M.; Losilla, E. R.; Sheptyakov, D. V.; Llobet, A.; Aranda, M. A. G. *Dalton Trans.* **2007**, *20*, 2058.
(15) León-Reina, L.; Losilla, E. R.; Martínez-Lara, M.; Bruque, S.; Aranda, M. A. G. *J. Mater. Chem.* **2004**, *14*, 1142.
(16) Ali, R.; Yashima, M.; Matsushita, Y.; Yoshioka, H.; Ohoyama, K.; Izumi, F. *Chem. Mater.* **2008**, *20*, 5203.
(17) Ali, R.; Yashima, M.; Matsushita, Y.; Yoshioka, H.; Izumi, F. *J. Solid State Chem.* **2009**, *182*, 2846.
(18) Tolchard, J. R.; Slater, P. R. *J. Phys. Chem. Solids* **2008**, *69*, 2433.
(19) Guillot, S.; Beaudet-Savignat, S.; Lambert, S.; Vannier, R. N.; Roussel, P.; Porcher, F. *J. Solid State Chem.* **2009**, *182*, 3358.
(20) Beaudet-Savignat, S.; Vincent, A.; Lambert, S.; Gervais, F. *J. Mater. Chem.* **2007**, *17*, 2078.
(21) Matsushita, Y.; Izumi, F.; Kobayashi, K.; Igawa, N.; Kitazawa, H.; Oyama, Y.; Miyoshi, S.; Yamaguchi, S. *Nucl. Instrum. Methods Phys. Res.* **2009**, *600*, 319.
(22) Kobayashi, K.; Matsushita, Y.; Igawa, N.; Izumi, F.; Nishimura, C.; Miyoshi, S.; Oyama, Y.; Yamaguchi, S. *Solid State Ionics* **2008**, *179*, 2209.
(23) Panteix, P. J.; Béchade, E.; Julien, I.; Abélard, P.; Bernache-Assollant, D. *Mater. Res. Bull.* **2008**, *43*, 1223.
(24) Kimura, T.; Yoshimoto, T.; Iida, N.; Fujita, Y.; Yamaguchi, T. *J. Am. Ceram. Soc.* **1989**, *72*, 85.
(25) Santacruz, I.; Porras-Vázquez, J. M.; Losilla, E. R.; Aranda, M. A. G. *J. Eur. Ceram. Soc.* **2011**, *31*, 1573.
(26) Kimura, T.; Holmes, M. H.; Newnham, R. E. *J. Am. Ceram. Soc.* **1982**, *65*, 223.
(27) Kaga, H.; Kinemuchi, Y.; Yilmaz, H.; Watari, K.; Nakano, H.; Nakano, H.; Tanaka, S.; Makiya, A.; Kato, Z.; Uematsu, K. *Acta Mater.* **2007**, *55*, 4753.
(28) Xiang, P. H.; Kinemuchi, Y.; Watari, K.; Ishiguro, H.; Cao, F.; Dong, X. L. *J. Mater. Res.* **2006**, *21*, 1830.
(29) Kajihara, M. *Acta Mater.* **2004**, *52*, 1193.
(30) Toropov, N. A.; Bondar, I. A.; Galakhov, F. Y. *Transactions of the 8th International Ceramics Congress*, Copenhagen, Denmark, 1962; p 85.
(31) Lotgering, F. K. *J. Inorg. Nucl. Chem* **1959**, *9*, 113.
(32) Bail, A. L.; Duroy, H.; Fourquet, J. L. *Mater. Res. Bull.* **1988**, *23*, 447.
(33) Izumi, F.; Momma, K. *Solid State Phenom.* **2007**, *130*, 15.
(34) Tanaka, S.; Kajihara, M. *J. Alloys Comp.* **2009**, *484*, 273.
(35) Putnis, A. *Introduction to Mineral Sciences*; Cambridge University Press: Cambridge, 1992.
(36) Johnson, D. *ZView Program*, Version 2.9b; Scribner Associates, Inc.: Southern Pines, NC, 1990.
(37) Bauerle, J. E. *J. Phys. Chem. Solids* **1969**, *30*, 2657.
(38) Marrero-López, D.; Canales-Vázquez, J.; Ruiz-Morales, J. C.; Rodríguez, A.; Irvine, J. T. S.; Núñez, P. *Solid State Ionics* **2005**, *176*, 1807.
(39) Irvine, J. T. S.; Sinclair, D. C.; West, A. R. *Adv. Mater.* **1990**, *2*, 132.
(40) Chesnaud, A.; Dezanneau, G.; Estournès, C.; Bogicevic, C.; Karolak, F.; Geiger, S.; Geneste, G. *Solid State Ionics* **2008**, *179*, 1929.
(41) Porras-Vázquez, J. M.; Losilla, E. R.; León-Reina, L.; Marrero-López, D.; Aranda, M. A. G. *J. Am. Ceram. Soc.* **2009**, *92*, 1062.
(42) Tao, S.; Irvine, J. T. S. *Mater. Res. Bull.* **2001**, *36*, 1245.
(43) Kim, Y.; Shin, D.-K.; Shin, E.-C.; Seo, H.-H.; Lee, J.-S. *J. Mater. Chem.* **2011**, *21*, 2940.
(44) Abram, E. J.; Sinclair, D. C.; West, A. R. *J. Mater. Chem.* **2001**, *11*, 1978.
(45) Huang, K.; Feng, M.; Goodenough, J. B. *J. Am. Ceram. Soc.* **1998**, *81*, 357.
(46) Huang, K.; Robin, S. T.; Goodenough, J. B. *J. Am. Ceram. Soc.* **1998**, *81*, 2565.
(47) Higuchi, Y.; Sugawara, M.; Onishi, K.; Sakamoto, M.; Nakayama, S. *Ceram. Int.* **2010**, *36*, 955.
(48) Abram, E. J.; Sinclair, D. C.; West, A. R. *J. Mater. Chem.* **2001**, *11*, 1978.
(49) Sansom, J. E. H.; Tolchard, J. R.; Slater, P. R.; Islam, M. S. *Solid State Ionics* **2004**, *167*, 17.
(50) Yoshioka, H. *Chem. Lett.* **2004**, *33*, 392.
(51) Kendrick, E.; Sansom, J. E. H.; Tolchard, J. R.; Islam, M. S.; Slater, P. R. *Faraday Discuss.* **2007**, *134*, 181.
(52) Yoshioka, H. *J. Am. Ceram. Soc.* **2007**, *90*, 3099.
(53) Kinoshita, T.; Iwata, T.; Béchade, E.; Masson, O.; Julien, I.; Champion, E.; Thomas, P.; Yoshida, H.; Ishizawa, N.; Fukuda, K. *Solid State Ionics* **2010**, *181*, 1024.